IOPscience iopscience.iop.org

Home Search Collections Journals About Contact us My IOPscience

Tunnel ionization of shallow acceptors and donors in GaAs

This article has been downloaded from IOPscience. Please scroll down to see the full text article.

1995 J. Phys.: Condens. Matter 7 2133

(http://iopscience.iop.org/0953-8984/7/10/020)

View the table of contents for this issue, or go to the journal homepage for more

Download details:
IP Address: 171.66.16.179
The article was downloaded on 13/05/2010 at 12:44

Please note that terms and conditions apply.

J. Phys.: Condens. Matter 7 (1995) 2133–2146. Printed in the UK

Tunnel ionization of shallow acceptors and donors in GaAs

A Dargys and S Žurauskas
Semiconductor Physics Institute, A Goštauto 11, LT-2600 Vilnius, Lithuania

Received 14 December 1994

Abstract. Experimental studies on shallow acceptor and donor field ionization dynamics in MBE-grown GaAs epitaxial layers are presented. The experiments have been carried out with a new non-resonant spectroscopic technique, transient tunnelling spectroscopy. It has been found that intense hole tunnelling from shallow acceptors begins at electric fields higher than 6000 V cm^{-1}, while electron tunnelling from shallow compensating donors to the conduction band occurs at much lower electric fields, of the order of 500 V cm^{-1}. The dependence of the acceptor to valence band tunnelling time on the electric field strength has been measured for the first time. From the analysis of the experimental results it is concluded that initially the acceptor to valence band tunnelling dynamics is dominated by a light-hole mass.

1. Introduction

Extremely high electric field intensities, in the range of megavolts per centimetre, are required to field ionize an atom in a vacuum. If the atom is in a semiconductor lattice, due to atom–lattice interaction, its ionization energy is reduced greatly. Especially drastic reduction occurs in case of the so-called shallow donors and acceptors. Since field ionization probability is an exponential function of atom ionization energy, a drastic reduction of a threshold electric field value for field ionization to begin is expected too. In spite of this fact, the quantum mechanical process of field ionization of donors and acceptors still remains poorly investigated, largely because other competing ionization mechanisms come into play long before impurity field ionization becomes important under normal experimental conditions. For example, impact ionization [1, 2, 3] by hot electrons and holes is rather strong at low lattice temperatures and moderate electric fields, firstly due to large donor and acceptor Bohr radius and secondly due to relatively large impurity atom concentrations, even in pure semiconductors, in comparison with atom concentrations used in experiments with atomic beams in a vacuum. Only recently, since the development of transient tunnelling spectroscopy (TTS), has it become possible to demonstrate unambiguously a manifestation of pure tunnelling as well as the transition from pure to phonon-activated electron tunnelling in doped semiconductors [4, 5]. In TTS the suppression of competing ionization mechanisms is achieved by using lightly doped samples, fast-ramped electric fields and reduced sample dimensions along the field direction.

In this paper we present the first experimental investigation on hole tunnelling from shallow acceptors to the valence band as well as electron tunnelling from shallow donors to the conduction band in GaAs under a variety of experimental conditions, for example, at various lattice temperatures and in the presence of either DC or pulsed free carrier injection. The electron injection into p-type material has allowed us to observe field ionization of compensating donors as well as field ionization of the main acceptor in the same sample.

0953-8984/95/102133+14$19.50 © 1995 IOP Publishing Ltd

The TTS technique has been described earlier [4]. However for better understanding of the present results we shall first summarize the principle of TTS and then describe the samples and experimental results.

2. Experimental procedure and samples

It is useful to draw a parallel between TTS and the well known deep-level transient spectroscopy (DLTS) [6]. TTS is based on tunnel rather than thermal ionization of impurities in semiconductors. In TTS, instead of lattice temperature, the voltage over the sample is scanned periodically. In contrast to DLTS, TTS is very fast. Its typical scanning time lies in the nanosecond time scale. The fast scanning at low temperatures allows us to eliminate all thermal ionization effects, and enables observation of pure quantum mechanical tunnelling. The equivalent measuring circuit is sketched in the upper part of figure 1. The p-type sample has the form of a thin platelet with two electrical contacts on the large faces. To exclude an injection of external carriers into the investigated volume of the sample during the scanning period, at least one of the contacts should be blocking. For measurement of the transient current the sample is connected in series with the load resistor R_L. In the present experiments the input impedance of the signal cable, $Z = 50\,\Omega$, served as the load resistor R_L. In figure 1(b) the ramped gate voltage V_g over the sample and the total transient current flowing through the sample, described as a ratio of the voltage drop V_L to the load resistor R_L, are drawn in the case of single impurity species. The total current consists of two parts, of the current plateau due to the charging of the geometrical capacitance of the sample and of the superimposed tunnelling current pulse I_t due to acceptor field ionization and subsequent hole drift to the collecting electrode. Figure 1(c) shows the energy diagram at some fixed moment. The reverse biased pn^+ junction (the gate voltage V_g is considered to be positive in this case) serves as a blocking contact with the heavily doped p^+ region as a collecting contact. The hole tunnelling from the acceptors to the valence band occurs in the p region. The drift of holes to the collecting electrode induces the transient current in the external circuit. To reduce distortions of a tunnelling spectrum it is important that the free carrier transit time through the p region be short in comparison with the characteristic tunnelling time. Then, the tunnelling current pulse shape will be dominated by acceptor to valence band tunnelling dynamics. The moment when the tunnelling pulse in the transient current appears is related directly to the acceptor level ionization energy and effective mass of the hole: the larger the ionization energy and/or effective mass are, the higher the electric field needed to ionize the acceptor and, consequently, the tunnelling pulse will appear at a later moment.

The studied n^+pp^+ samples were grown in a standard three-chamber molecular beam epitaxial system (MBE) with a semihorizontal arrangement of the sources. The heavily doped, (100)-oriented n^+-type GaAs wafer was precoated with a 0.7 μm thick n^+-type GaAs buffer layer and then the investigated 13 μm thickness layer of undoped p-GaAs was grown at the rate of about 3 $\mu m\,h^{-1}$ at substrate temperature 600 °C. Finally the heavily doped 0.9 μm p^+-GaAs gate cap layer was grown for ohmic contact. From the earlier growth experience with the MBE apparatus, the prevailing residual acceptor is known to be the carbon which is a dominant residual acceptor in high-purity MBE samples. The samples of an area less than 1 mm^2 were cleaved from the wafer. The indium used to mount the wafers to the sample holder during the MBE growth was not removed and served as an ohmic contact to the n^+ substrate. An indium pin mildly pressed over the p^+ cap layer served as a gate electrode. Table 1 lists the parameters of samples used in the present

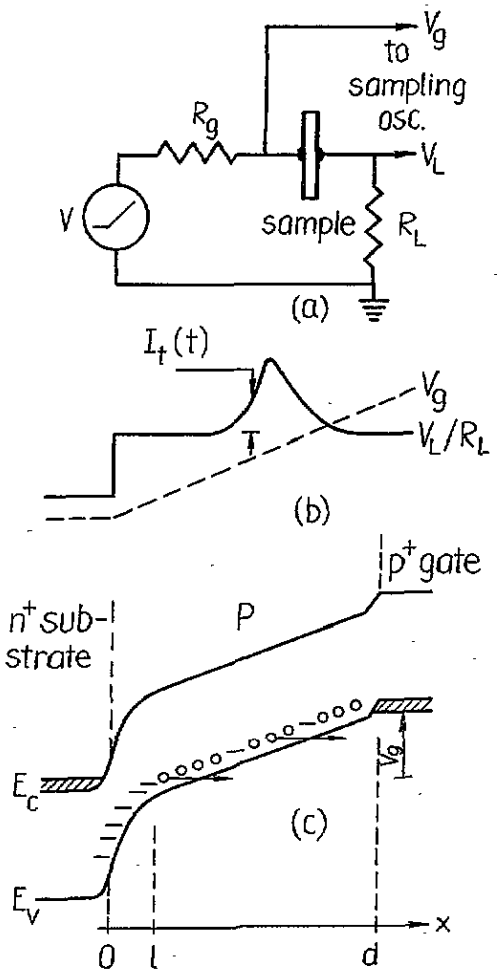

Figure 1. The principle of TTS for measurement of the acceptor field ionization dynamics. (a) Equivalent scheme: R_L is the load resistor and R_g is the generator equivalent output resistance. (b) Voltage ramp applied to the gate electrode and the resulting transient current, $I_t = V_L/R_L$, in the case of a single acceptor. (c) Energy band diagram at a fixed moment.

work. The hole concentration, which varied from 2 to $4\times10^{14}\,\mathrm{cm}^{-3}$, was determined from C–V curves at room temperature.

3. Experimental results

In all cases the voltage drop over the load R_L made up only a small fraction of the voltage V_g applied to the gate electrode, thus to a good accuracy one may assume that the voltage over the sample equals V_g. The evolution of the tunnelling spectrum with increasing gate voltage rate is shown in figure 2 for sample B1-8 at liquid helium temperature. The capacitive current is proportional to the slope of the voltage on the gate electrode. Its magnitude is in a good agreement with that calculated from the sample capacitance and voltage time derivative. In the spectra one can resolve two overlapping tunnelling peaks superimposed

Table 1. Properties of the epitaxial p-GaAs samples. N_a is the total acceptor concentration found from C–V characteristics at 300 K; S is the area and d is the thickness of the epitaxial p layer; l is the depletion layer width; Q_1/Q_2 is an approximate ratio of areas under the first and second acceptor tunnelling peaks; α_C and Ω_C are the tunnelling parameters of the carbon acceptor (see expression (3)). τ_{rC} is carbon tunnelling time calculated with (3) at the electric field amplitude 6.5 kV cm^{-1}.

Sample	N_a (10^{14} cm^{-3})	S (mm^2)	d (μm)	l (μm)	Q_1/Q_2	α_C (kV cm^{-1})	Ω_C (10^{12} s^{-1})	τ_{rC} (10^{-9} s)
B1-3	2.7	0.83	13	2.8	1/1	55	0.3	16
B1-4	3	0.5	13	2.7	1/1	73	4	19
B1-5	3	0.56	13	2.7	1/1	60	0.3	34
B1-6	4	0.6	13	2.3	1/1	74	4	22
B1-7	2	0.75	13	3.3	1/2	69	0.7	58
B1-8	2	0.73	13	3.3	1/2	48	0.07	23

on the capacitive current. As the gate voltage rate is increased both peaks appear earlier and become narrower which suggests that the acceptor to valence band tunnelling depends on the instantaneous value of the electric field in the p region. As seen from the figure the tunnelling becomes very efficient when average electric field $\bar{F} = V_g/d$ in the p-type region reaches about 6 kV cm^{-1} (arrows in figure 2). The total number of acceptors in the p region depends on the depletion layer width l as shown in figure 1. The latter can be changed by applying an additional DC bias voltage V_b on the gate electrode:

$$l = \left[\frac{2\epsilon_0\epsilon_r(V_b + E_g)}{eN_a^-}\right]^{1/2}. \tag{1}$$

In (1) ϵ_0 and ϵ_r are the electrical constant and the lattice relative permittivity, respectively, E_g is the band gap energy in volts, N_a^- is the ionized acceptor density. Figure 3 illustrates the variation of the spectrum when either negative or positive DC bias is applied to the gate electrode. The positive bias reduces the number of neutral acceptors in the p region, as a result, the tunnelling pulse amplitude becomes smaller. An opposite situation is observed in the case of a negative bias. However, a drastic transformation in the spectrum takes place when the negative bias, as seen from figure 3(a), exceeds E_g. In the latter case the leading edge of the tunnelling pulse shifts to earlier times and a new pulse appears at $t \approx 0$. The detailed structure of the new pulse is displayed in figure 4. Now, depending on the bias, one can notice that the new pulse is made up either of one or of two peaks. The first peak is associated with free carriers, i.e. with free electrons and holes injected into the p region from p^+ and n^+ contacts when $|V_g| > E_g$. The second peak is connected with field ionization of shallow donors that have been neutralized by the injected electrons. The transition from one peak to two peaks with the increase of the bias amplitude can be explained in the following way. At small negative bias, when the pn^+ junction just opens, the number of injected free electron and holes in the p region is small. Most of them are trapped by ionized acceptors and compensating donors. In this case one observes the growth of the second, i.e. donor to conduction band tunnelling peak, with the bias amplitude. Since the ionization energy of shallow donors is smaller than the acceptor ionization energy, the donor peak appears at lower fields, 500 V cm^{-1} $< \bar{F} <$ 1000 V cm^{-1}. At high injection level the DC electric field in the p region becomes high enough to ionize donors by impact ionization. As a result, quenching of the donor peak is observed. At the same time with the increase of the injection level the free carrier peak grows. Figure 5 shows the effect of lattice temperature on the donor to conduction band tunnelling peak at the fixed bias $V_b = 2$ V. The amplitude of the

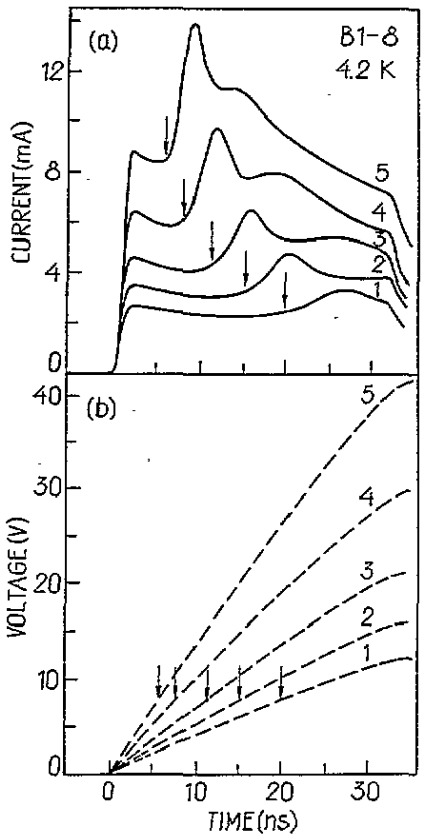

Figure 2. (a) The tunnelling spectrum for sample B1-8 at different voltage ramp rates; the arrows indicate the moment when the electric field in the p layer reaches $6\,\mathrm{kV\,cm^{-1}}$. (b) Time dependence of the gate voltage; the numbering of curves is the same as in (a).

peak, as seen, decreases as the sample temperature is raised. The inset in the same figure shows electron concentration on the donors, $n_d = 2Q/(edS)$, deduced from the charge Q under the peaks as a function of inverse lattice temperature. The area under the peaks is referred to the dashed line that represents a high-temperature limit. The solid line in the inset has been calculated from a balance equation between emission and capture processes discussed in more detail in the next section. An overall view of the tunnelling spectrum of the sample B1-6 at zero bias and five fixed sample temperatures is shown in figure 6. The spectrum changes insignificantly up to 20 K. This indicates that phonon influence on the tunnelling dynamics in the investigated material is insignificant in this temperature range. At higher temperatures, in the range from 20 to 40 K, the free hole pulse appears; as a result, in between the free hole pulse and the tunnelling pulse a valley develops. The valley narrows down with the lattice temperature. This can be explained in the following way. The extraction of thermally generated free holes at the first moments of the voltage ramp leaves ionized acceptors which results in an increase of the electric field value near the pn^+ junction. This and, probably, phonon participation in the tunnelling process at elevated temperatures shifts the tunnelling peak to earlier times and narrows the valley. At $T \geqslant 40\,\mathrm{K}$ nearly all acceptors are already ionized by lattice vibrations. At these temperatures the shape of the transient current is completely determined by the growth of the depletion layer due

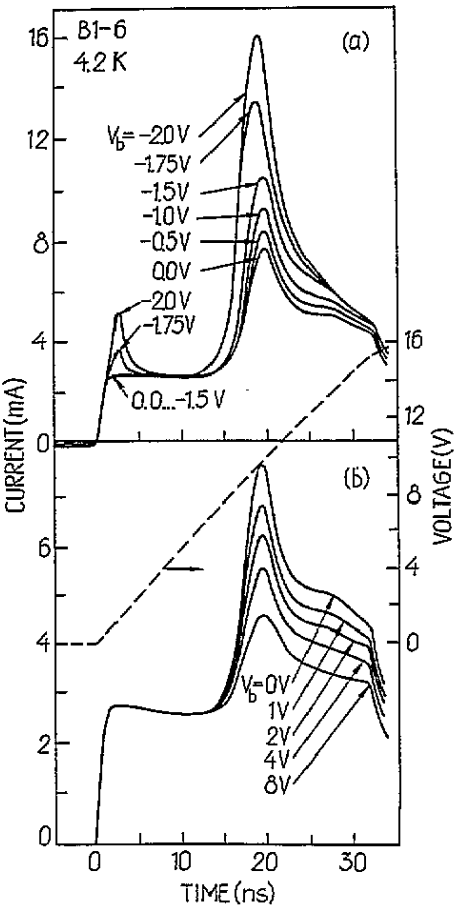

Figure 3. The tunnelling spectrum at different DC biases V_b applied to the gate electrode of sample B1-6 at $T = 4.2$ K. (a) Accumulation bias. (b) Depletion bias.

to extraction of free holes by the ramp. The presence of two hole peaks in the spectra can be associated either with the presence of two different impurity species having different ionization energies or with the complex valence band structure characterized by light and heavy hole masses. Below we shall describe an additional experiment that sheds light on the origin of the second peak. The experiment makes use of the facts that (i) the thermalization rate of hole population on the acceptor level after termination of a perturbation depends on the acceptor ionization energy and (ii) the thermalization rate is slow in comparison with the field ionization rate. Therefore, if two different acceptors have different ionization energies then thermalization is expected to take place with different time constants. Figure 7 demonstrates such results. The sample temperature has been raised to 20 K, so that the energy level population associated with the first peak has enough time for thermalization. Then, the sample has been shortly perturbed by applying a negative-polarity-injecting bias pulse to the gate electrode. Finally, after some delay t_d, the voltage ramp has been applied to the sample (see inset in figure 7). From the spectra obtained in this way one can see that for all delays the first peak remains unperturbed; however, the second peak slowly relaxes to the unbiased value. This unambiguously indicates that in this case we have to do

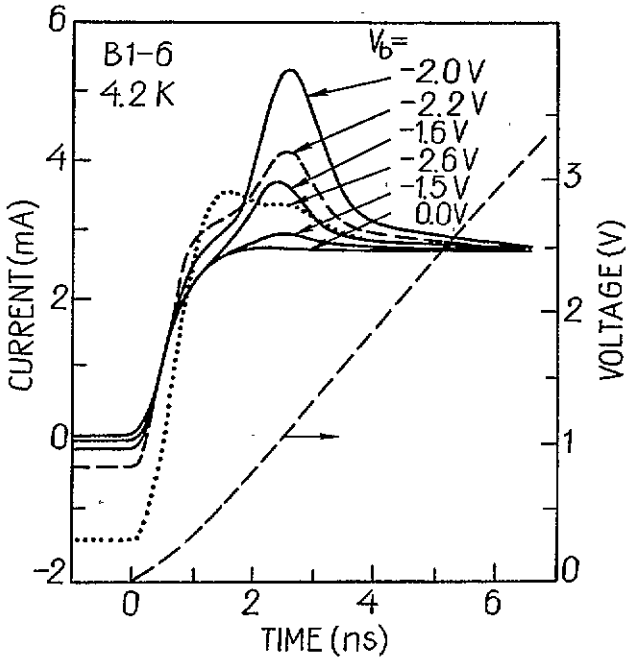

Figure 4. The detailed structure of the initial part of the spectrum in figure 3(a). Notice the development and quenching of the second (donor) peak with the growth of the bias amplitude V_b.

with two, different levels, which have different ionization energies. The low-temperature photoluminescence spectrum obtained on the same wafer at liquid helium temperature has confirmed the presence of two dominating acceptors in our samples [7]. The shallowest acceptor has been found to be connected with carbon atoms while the second, deeper one with the d_n acceptor-like 'defect complexes' [8], the concentration of which in MBE GaAs is known to be comparable to carbon concentration.

4. Analysis of the results

4.1. Tunnelling from carbon acceptor

At the leading edge of the first tunnelling peak, where the tunnelling current increases exponentially, the number of field-ionized carbon acceptors in the p region is small. At these initial moments space charge effects may be neglected, and as shown earlier by us [9] the analysis greatly simplifies in this case. However, at later moments, when the growth rate of the current slows down and finally the maximum is reached, the deviation from a uniform electric field distribution due to ionized acceptor space charge becomes significant. A full numerical analysis, including Poisson's equation, should then be addressed [9]. In the following the leading edge of the first tunnelling peak, where space charge effects are unimportant, is analysed and the dependence of the tunnelling time on the electric field is deduced. In the appendix it is shown that under our experimental conditions the impact ionization by free carriers is unimportant during the fast voltage ramp.

In the limit of thin p region width, when the free hole transit time through the p region

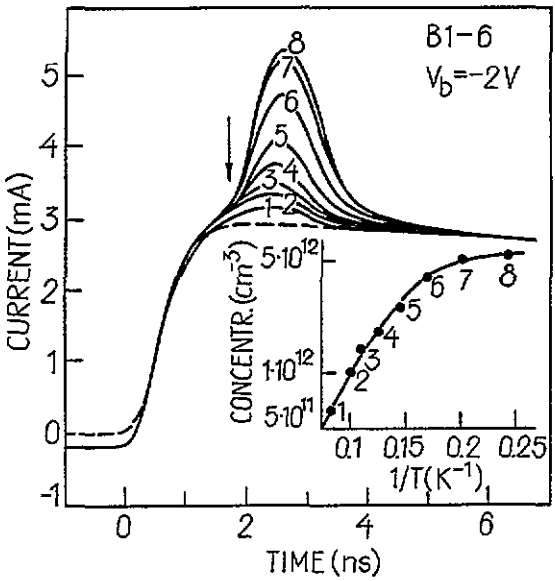

Figure 5. *Evolution of the donor peak with lattice temperature at the fixed bias* $V_b = 2$ V. *The* dashed line is for reference. The voltage ramp is the same as in figure 4. The arrow indicates the moment when electric field is 500 V cm^{-1}. The inset shows the electron concentration on the donors deduced from the area under the donor peaks as a function of the inverse temperature.

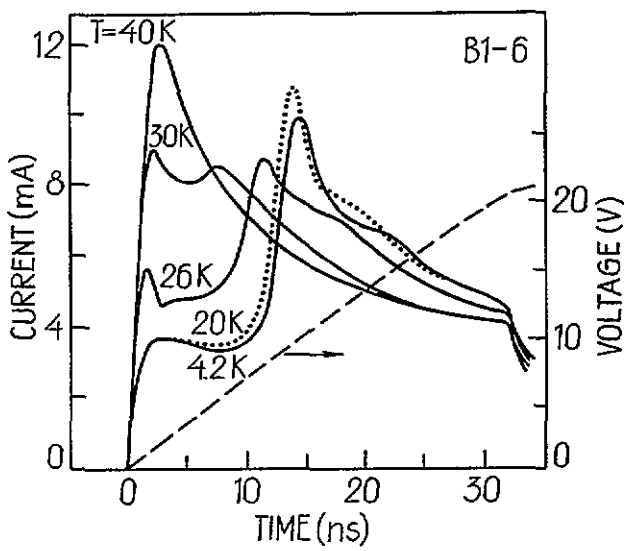

Figure 6. Evolution of the transient current pulse when the sample temperature is increased from 4.2 to 40 K.

is much shorter than the tunnelling time τ_t, and when the uniform electric field distribution is only slightly perturbed, using the continuity and rate equations one can show that the tunnelling current density is

$$J_t \approx -\frac{ed}{2}\frac{\mathrm{d}\,p_a}{\mathrm{d}t} \approx \frac{ed}{2}\frac{N_a}{\tau_t}. \tag{2}$$

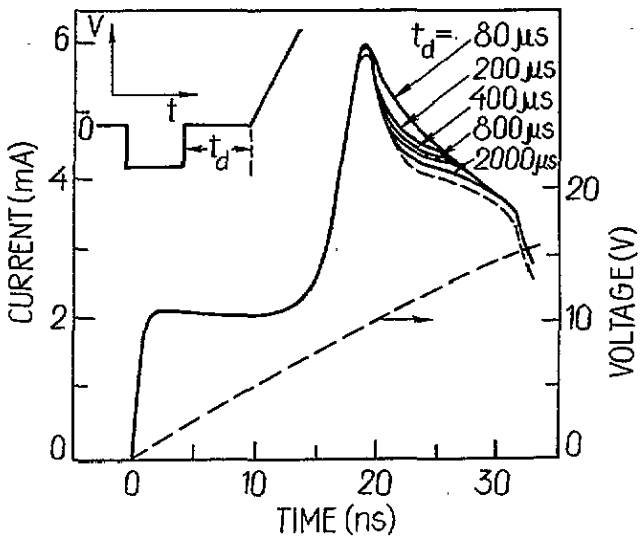

Figure 7. Dependence of spectrum on the delay time t_d between pulsed bias and leading edge of the ramp (see the inset). The dashed spectrum corresponds to zero bias.

Here p_a is the concentration of holes on the acceptors (concentration of neutral acceptors). Equation (2) has a very clear interpretation: dN_a/τ_t is the number of free holes per unit area and unit time that appears in the valence band. The factor $\frac{1}{2}$ takes into account the average free hole transit length in the p region. In the following analysis a standard exponential dependence of the tunnelling time on the electric field F will be assumed

$$\tau_t = \Omega^{-1} \exp(\alpha/F). \tag{3}$$

In the general case, the attempt to escape frequency Ω is a function of electric field. For simplicity we shall assume that Ω is a constant. Then with (2) and (3) one can write with respect to F an Arrhenius-type equation

$$\ln J_t = \gamma - \alpha/F \tag{4}$$

where $\gamma = edN_a\Omega/2$. If depletion length l cannot be neglected then N_a should be replaced by $\bar{N}_a = N_a(1 - l/d)^2$.

In figure 8 the Arrhenius-type plots of the leading edges are shown for samples B1-8 and B1-6. The electric field in the p region at the moment t has been calculated from $\bar{F}(t) = V_g(t)/d$. Different symbols correspond to different average electric field rates $d\bar{F}/dt$ in the range from 2.5×10^{11} to 10^{12} V cm^{-1} s^{-1}. Figure 8(a) and (b) corresponds to two extreme cases, i.e. it represents the largest and the smallest divergence of the experimental points from the Arrhenius line. No correlation has been observed between the points in figure 8 and the rate of change of V_g. The tunnelling parameters α and Ω deduced from the averaged Arrhenius plots are summarized in table 1. In finding Ω the finite width of the depletion layer has been taken into account (see text after (4)) and the acceptor concentration has been used that corresponds to the first peak (see table 1). As can be inferred from table 1 there is a strong correlation between α and Ω values deduced in the above-described way; the larger α is, the larger the corresponding Ω value is. However, as can be seen from the last column in table 1, the scatter of the tunnelling times calculated with (3) and α and Ω values in table 1 is smaller. Therefore, to minimize the error we have summarized the dependence of τ_t on F in figure 9 in the form of a hatched band using the corresponding

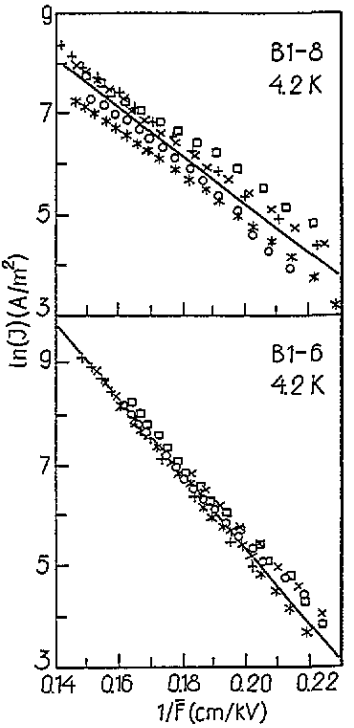

Figure 8. Arrhenius plots of the leading edges of the tunnelling pulses for two samples. Different symbols correspond to different rates of the ramped gate voltage. The straight lines are calculated with (4) and parameters in table 1.

pairs of α and Ω values of six samples given in table 1. Theoretically hole tunnelling from acceptors to the valence band has been considered in [10], where it has been concluded that due to heavy- and light-hole subband mixing by the electric field the light-hole mass basically will dominate the tunnelling process. In figure 10, curve 1 shows the transient tunnelling current calculated with the help of Poisson, current continuity and rate equations as described in detail in [5]. The acceptor to valence band tunnelling rate was taken from [10] assuming that the parameter γ in formula (5.2) of [10] is equal to zero:

$$\tau_t^{-1} = \omega \left(\frac{6\alpha}{F}\right)^{2n_l^*-1} \exp\left(-\frac{\alpha}{F}\right) \tag{5}$$

where

$$\omega = \frac{1}{\sigma^2[\Gamma(n_l^*+1)]^2}\frac{2\mid E_i \mid}{\hbar} \tag{6}$$

$$\alpha = \frac{4(2m_l^*)^{1/2}E_i^{3/2}}{3e\hbar} \tag{7}$$

$$n_l^* = \frac{e^2}{4\pi\epsilon_0\epsilon_r\hbar}\sqrt{\frac{m_l^*}{2E_i}}. \tag{8}$$

The following parameter values were used in (6)–(8). The light-hole mass m_l^* was taken in the direction of the electric field $F \parallel \langle 100\rangle$, $m_l^* = 0.0905m_0$. E_i was assumed to be equal

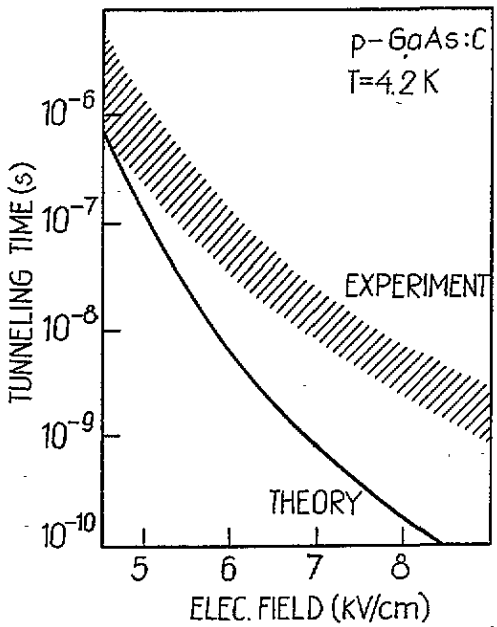

Figure 9. Dependence of the carbon acceptor to valence band tunnelling time on electric field strength. The hatched band is the present experiment. The solid line is the theory [10].

to the activation energy of the carbon, $E_i = 26\,\text{meV}$. σ^2 is related to parameters which characterize the valence band, $\sigma^2 = 0.66$. ϵ_r is the relative lattice permittivity, $\epsilon_r = 12.8$. The other notations are standard. Curve 1 in figure 10 shows that efficient tunnelling begins at an average electric field $V_g/d = \bar{F} > 5\,\text{kV cm}^{-1}$, i.e. at electric field slightly smaller than that observed experimentally. For comparison, in the same figure we have also plotted the transient current when in the calculation of the tunnelling rate, (5)–(8), instead of light-hole mass, the heavy one ($m_h^* = 0.377m_0$) is inserted (curve 2). Now, the acceptor field ionization begins at a threshold field that is much higher than that found in the experiment. From expressions (6)–(8) one gets the following tunnelling parameters for carbon impurity: $\omega = 1.8 \times 10^{14}\,\text{s}^{-1}$, $\alpha = 86\,\text{kV cm}^{-1}$ and $n_1^* = 0.55$. The solid line in figure 9 is calculated with (5) and these parameters. In our case the factor $(6\alpha/F)^{2n_1^*-1}$ in (5) is close to unity; for this reason the above-calculated α and ω values could be directly compared with α_C and Ω_C in table 1. As seen, the experimentally measured tunnelling parameters are systematically lower than the calculated ones. The discrepancy between theory and experiment may be conditioned by a number of factors, for example, by neglect of the splitting of the fourfold-degenerate acceptor level and valence band edge due to either residual strains in the sample or the Stark effect [11, 12], or by neglect of admixture of the heavy-hole wavefunction in the tunnelling rate [10]. At this stage it is difficult to assess the relative importance of these additional factors.

4.2. Tunnelling from shallow donors

The peaks in figure 5 appear at low DC injection current level and are associated with field ionization of shallow compensating donors that have been partly neutralized by injected electrons from n^+ contact. All peaks appear at electric field higher than $500\,\text{V cm}^{-1}$, the

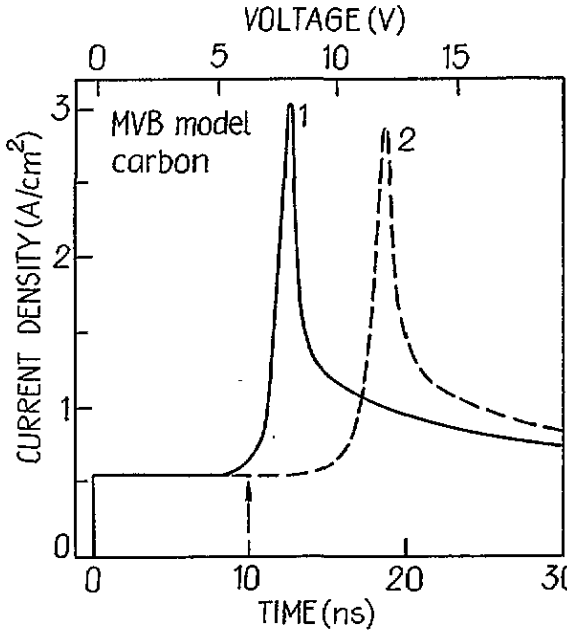

Figure 10. The spectra calculated with the MVB model when a single carbon acceptor level is taken into account. Curves 1 and 2 correspond to light- and heavy-hole masses. The arrow indicates the moment when average electric field, $\bar{F} = V_g/d$, in the p layer reaches 5 kV cm^{-1}.

threshold value which is expected from simple scaled hydrogenic model considerations. Below we shall analyse the temperature dependence of the area under the donor peak.

In the intervals between field ionizing ramps the number of electrons trapped by donors is determined by three processes: (i) electron capture by ionized donors with a characteristic time constant τ_C, (ii) electron emission back to the conduction band due to thermal ionization with a characteristic time constant τ_T, and (iii) electron emission to the conduction band due to the presence of the DC bias electric field, for example due to impact ionization, with a characteristic time constant τ_F. If n and n_d are electron densities in the conduction band and on the donors, then in between the ramps the concentration n_d changes according to

$$\frac{dn_d}{dt} = \frac{n}{\tau_C} - \frac{n_d}{\tau_T} - \frac{n_d}{\tau_F}. \tag{9}$$

Assuming that τ_C and τ_T are approximately related by the detailed balance equation, from (9) it follows that in the steady state

$$n_d = \frac{n}{(N_c/gN_d)\exp(-E_d/kT) + \tau_C/\tau_F} = \frac{C_1}{C_2\exp(-E_d/kT) + 1}. \tag{10}$$

In (10) N_c and N_d are the density of states in the conduction band and the compensating donor concentration, respectively. E_d is the donor activation energy. The solid line in the inset of figure 5 is calculated with (10) and $C_1 = n\tau_F/\tau_C = 5.74 \times 10^{12}\,\mathrm{cm}^{-3}$, $C_2 = (\tau_F N_c)/(\tau_C g N_d) = 200$ and $E_d = 3.2\,\mathrm{meV}$.

The shallow impurity ionization energy E_d depends on the impurity concentration. In case of shallow donors in n-type GaAs, E_d is given by the approximate formula [13]:

$$E_d\ (\mathrm{meV}) = 6 - 2.2 \times 10^{-5}(N_d\ (\mathrm{cm}^{-3}))^{1/3}\ . \tag{11}$$

Equation (11) is expected to remain a good approximation for donors in p-type GaAs as well. Inserting $N_d = 2 \times 10^{14}\,cm^{-3}$ (this value corresponds to compensation ratio $N_d/N_a = 0.5$) in (11) one obtains that $E_d = 4.7\,meV$. This value is somewhat higher than E_d found from figure 5. From C_2 one can estimate that the ratio τ_F/τ_C is about 16, and then from C_1 calculate the injected free electron concentration: $n = 3.5 \times 10^{11}\,cm^{-3}$. This value is consistent with the value found from DC injection current I_{inj} in figure 5 at $t < 0$, if a reasonable value of drift velocity, $v = 10^6\,cm\,s^{-1}$, is used: $n = I_{inj}/(evS) = 2.6 \times 10^{11}\,cm^{-3}$.

5. Conclusions

The tunnelling of holes from acceptors to the complex valence band of p-type GaAs has been observed for the first time. Undoped, 13 μm thickness MBE-grown epitaxial layers, thinner by nearly an order than in our previous experiments with n-type Si and Ge [4, 5], have been used for this purpose. This has allowed us to eliminate completely the interfering effect of impact ionization by hot carriers [3]. The acceptor to valence band tunnelling process in p-GaAs is found to predominate at electric fields higher than $6\,kV\,cm^{-1}$. The characteristic behaviour of the tunnelling spectra with DC bias and lattice temperature indicates unambiguously that we, indeed, observe pure quantum mechanical tunnelling from acceptors to valence band. The tunnelling process is dominated by light holes. No specific structure associated with the complex valence band could be resolved in the hole tunnelling spectrum. From the analysis of the leading edge of the tunnelling spectra, where influence of the field distortions in the sample are unimportant, the hole tunnelling time from carbon acceptor to valence band has been measured. The second hole tunnelling peak, which appears at higher electric fields, has been found to be associated with a deeper acceptor.

By using double injection from electrical contacts we have managed on the same samples to observe electron tunnelling from shallow compensating donors into the conduction band at electric fields that are lower by an order than those needed for acceptor field ionization. In earlier experiments [3] we have observed that under normal experimental conditions, i.e. in comparatively long and moderately doped n-type GaAs samples, the donor avalanche breakdown due to impact ionization of neutral donors sets up at lower electric fields, of the order of $10\,V\,cm^{-1}$. In the present samples the donor impact ionization does not develop since, first of all, the samples are short and, secondly, only a small fraction, about 3%, of the compensating donors has been neutralized and then field ionized.

Acknowledgments

The authors are thankful to Dr K Bertulis for growing p-GaAs epitaxial layers. The research described in this publication was made possible in part by grant no U5Q000 from the International Science Foundation.

Appendix

Impact by a free hot carrier is one of the important mechanisms by which an impurity can be ionized at high electric fields and low lattice temperatures. This mechanism is very effective in long samples doped with shallow impurities. For the full development of impact ionization the distance between the contacts must be larger than some characteristic length,

called the impact ionization length:

$$l_{\mathrm{I}} = v/(A_{\mathrm{I}} N_{\mathrm{a}}) \ . \tag{A1}$$

Here A_{I} is the impurity impact ionization coefficient. The dependence of A_{I} on electric field strength for n-GaAs as well as for other materials has been measured in [3]. For p-GaAs the dependence of A_{I} on the electric field strength is unknown. Usually A_{I} is a strong function at low electric fields and saturates at high fields. According to [3] for shallow impurities a typical saturation value of A_{I} in various semiconductors in the high-electric-field range is $10^{-5}\,\mathrm{cm}^{-3}\,\mathrm{s}^{-1}$. Then, assuming that $N_{\mathrm{a}} = 2 \times 10^{14}\,\mathrm{cm}^{-3}$, $v = 2 \times 10^{7}\,\mathrm{cm\,s}^{-1}$, from (A1) it follows that $l_{\mathrm{i}} \approx 100\,\mu\mathrm{m}$. Thus, the impact ionization length in our samples is larger by an order than the p region length. The unimportance of the impact ionization in our experiments can also be noticed from figure 3: the variation of the neutral layer width by the DC bias voltage affects only the amplitude of the tunnelling peak, and not the location of the peak on the time axis. Similar considerations also hold for the neutralized compensating donors in our samples. Thus, we conclude that under our experimental conditions the impact ionization is unimportant.

References

[1] Robbins D J and Landsberg P T 1980 *J. Phys. C: Solid State Phys.* **13** 2425

[2] Peinke J, Parisi J, Rössler O E and Stoop R 1992 *Encounter with Chaos. Self-Organized Hierarchical Complexity in Semiconductors* (Berlin: Springer)

[3] Dargys A, Česna A and Kundrotas J 1992 *Semicond. Sci. Technol.* **7** 210

[4] Dargys A, Žurauskas S and Žurauskienė N 1991 *Appl. Phys.* A **52** 13

[5] Žurauskas S, Dargys A, and Žurauskienė N 1992 *Phys. Status Solidi* b **173** 647

[6] Lang D V 1974 *J. Appl. Phys.* **45** 3023

[7] Česna A, Bertulis K, Dargys A and Kundrotas J 1994 *Lietuvos Fizikos Žurnalas* **46** 499

[8] Szafranek I, Plano M A, McCollum M J, Stockman S A, Jackson S L, Cheng K Y and Stillman G E 1990 *J. Appl. Phys.* **68** 741

[9] Dargys A, Žurauskas S and Žurauskienė N 1987 *Lietuvos Fizikos Rinkinys* **27** 322 (Engl. Transl. *Sov. Phys. Collection* **27** 66)

[10] Hui-Quan Nie and Coon D D 1984 *Solid State Electron.* **27** 53

[11] Ishiguro T 1973 *Phys. Rev.* B **8** 629

[12] Dargys A, Žurauskas S and Žurauskienė N 1993 *Acta Phys. Pol.* A **84** 629

[13] Dargys A and Kundrotas J 1994 *Handbook on Physical Properties of Ge, Si, GaAs and InP* (Vilnius: Science and Encyclopedia Publishers)